Fall 2021

Research and development of a laser hot wire deposition process

Christopher Croft

Department:

RESEARCH AND DEVELOPMENT OF A LASER HOT WIRE DEPOSITION PROCESS

by

CHRISTOPHER CROFT

A THESIS

Presented to the Graduate Faculty of the

MISSOURI UNIVERSITY OF SCIENCE AND TECHNOLOGY

In Partial Fulfillment of the Requirements for the Degree

MASTER OF SCIENCE

in

MANUFACTURING ENGINEERING

2021

Approved by:

Dr. Frank Liou, Advisor
Dr. Todd Sparks
Dr. Ashok Midha

ABSTRACT

Laser hot wire directed energy deposition (DED) is an increasingly popular method for improving deposition rates and overall reduction of build times in DED processing. While there is clear benefit, it is important to fully understand the impact of preheating the wire. This work focuses on developing a model that describes bead geometry output using all factors including the wire preheat. The model was fit with over 150 data points that explored a large range of each factor. The resulting model was then leveraged to evaluate a process control variable. The technique chosen used feedback from the hot wire system to modulate travel speed and control deposition height. Experiments were performed and analyzed that showed the efficacy of the control technique. Finally, a case study explored potential benefits of having an in-control process and a deep understanding of the parameter space. While this work focuses on laser hot wire DED, the tools presented aim to lay a foundation for advancing the science of thermal processes.

ACKNOWLEDGMENTS

This work was supported by GKN Aerospace through the Center for Aerospace Manufacturing Technologies (CAMT) and the Intelligent Systems Center (ISC) at Missouri S&T. Their financial support is greatly appreciated.

TABLE OF CONTENTS

Page

LIST OF ILLUSTRATIONS

LIST OF TABLES

Table Page

1. INTRODUCTION & BACKGROUND

Directed Energy Deposition (DED) is an Additive Manufacturing (AM) technique that uses a feed stock material, primarily metal, and an energy source to build parts layer-by-layer [27]. A common metal AM method called DED laser wire uses laser as the energy source and a metal wire as the feed stock. The method has existed for decades under many different names, most commonly laser metal deposition (LMD), and will be the focus of this work [9]. An example of this process, from Missouri University of Science and Technology, is shown in Figure 1.1.

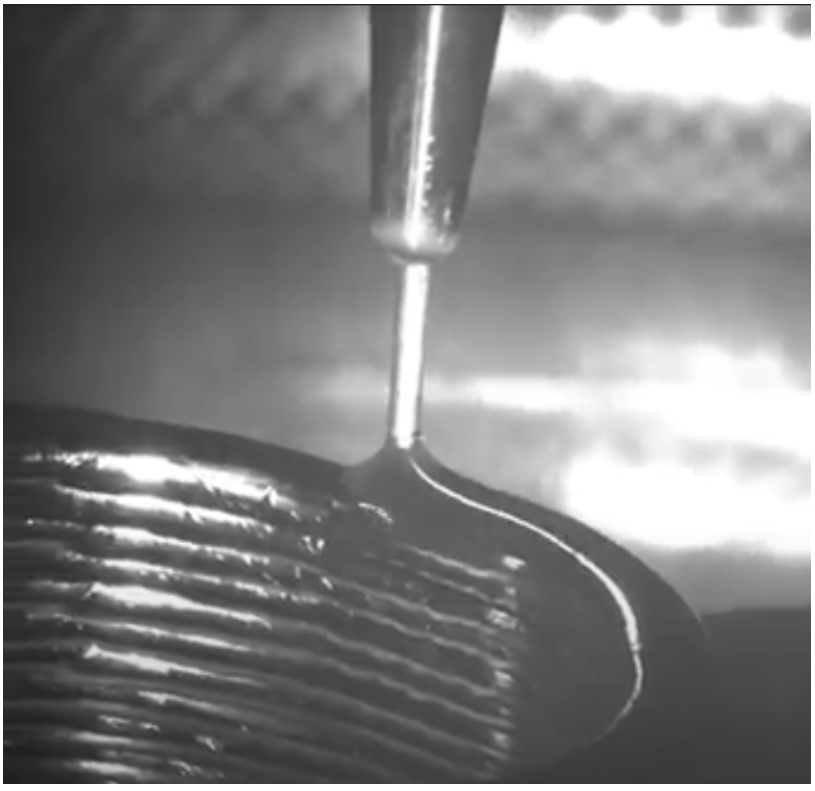

Figure 1.1. DED Laser hot wire process as seen by a Cavitar Welding Camera

In recent years, metal AM methods have began to progress from research and development into production. This is mainly feasible due to the improvements in technology and the drop in startup cost and technical capability necessary to operate the equipment.

Current cost estimates range DED equipment from $200k up to over $2 million. Lower material costs puts titanium DED at $2.37 per cubic centimeter [8]. With lower costs, large industries like aerospace, military, and automotive have increased investment into AM technology and its research. In-process monitoring, and control improvements aim toward the goal of qualification and certification of AM technologies. Which consists of qualification and certification of not only the material, but the process and the equipment used for the process. These include the energy source, in-process measurements, defect detection technologies, and material testing specifications [1]. As the technology improves, material specifications evolve that seek to regulate the AM material produced for the growing market. The original material specification for DED titanium for aerospace applications is SAE AMS4999, which is the most relevant to this work. Requirements such as material composition, deposition practices, thermal processing, and material performance are detailed in these documents [2].

There are many areas for DED technology and capability to improve and evolve. The focus of this work tackles both monitoring and control of the process. Using feedback from the process in the control loop simultaneously tracks what is occuring in the system and keeps the deposition in-control. This helps achieve the goals outlined above by increasing reliability and repeatability in the AM parts, while capturing in-situ data. Additionally this work looks at modeling of the DED process, another thrust area in AM technology [1].

2. LITERATURE REVIEW

Laser hot wire has been used as a welding technique for decades as well. In 1992, Phillips and Metzbower used laser hot wire to weld HY80 and HY100 steels [22]. Kottman et al. demonstrated the feasibility of laser hot wire applied to additive manufacturing in 2015. The process is described as adding secondary resistive heating of the wire to a DED process with benefits of reduced quenching effect, increased productivity, and a reduction in superheat necessary to ensure complete melting of the wire. This showed the process's capability to produce Ti-6Al-4V for aerospace applications as well as tool steel and others [18]. This section will provide evidence of these potential benefits and discuss the state of the art for the technology.

2.1. LASER HOT WIRE AND WIRE ARC TO DATE

As mentioned earlier, hot wire has the capability to increase deposition rate over a cold wire system. It also has many similarities to wire arc systems. Each of these is discussed in the following sections.

2.1.1. Hot Wire. Bambach et al. found in a comparison of cold wire and hot wire that each process was capable of depositing 0.600 and 0.876 kg/hr respectively [5]. Gibson et al. mention that the work cell used during development of melt pool size control used a hot wire system that "supplied relatively low-power auxiliary resistance heating of the wire" and the resulting deposition rate was 2.4kg/hr for Ti-6Al-4V [12].

Thermal stresses in metal AM parts have always been a concern since they can cause part distortion depending on the heat input to the part and the coefficient of thermal expansion (CTE) of the material [9]. Germain et al. assessed residual stresses in powder bed AM titanium and found that heating the plate to 600°C for 2 hours could relieve most of the stresses from the process [11].

Liu et al. found that using hot wire over cold wire allowed for complete filling of a 1 mm gap during butt welding of 9.5 mm thick A36 steel with a reduced overall heat input of 15.5% [20]. Wei et al. found a similar result at 16% energy savings while welding DP800 steel [34].

2.1.2. WAAM. Wire Arc Additive Manufacturing (WAAM) is a DED method that uses traditional wire arc welding methods to build parts layer by layer. While the process is similar, each has its own advantages. WAAM has significantly lower costs to laser processes. However, using a laser allows for faster cooling rates and lower overall heat input into the part. This is because the nature of the WAAM process conducting through the part to the weld lead. A comparison of Ti-6Al-4V on both processes showed reduced HAZ, residual stress, and finer microstructure in the DED process [28]. Brandl et al. did a comparison of WAAM and LMD-w for Ti-6Al-4V in the context of aerospace material specifications. It was found that both processes were capable of producing properties exceeding values of wrought, but each had advantages for different tests and therefore either could be more beneficial depending on the application. Aerospace components that are candidates for being produced with AM are typically being used in fatigue applications, so those properties are emphasized [7].

2.2. BEAD GEOMETRY MODELING

Numerical modeling is a popular tool used to understand and explain experiments and results. Kanigalpula et al. looked at bead width and penetration in an electron beam welding (EBW) process. A regression model was fit from a central composite design (CCD) experiment. This model allowed researchers to minimize the area of the weld bead while maintaining the integrity of the weld and minimizing heat affected zone (HAZ) [15]. Olshanskaya et al., used regression analysis to fit another EBW process to the shape of the weld bead to find a balance of penetration depth and weld defects [21]. Walker et al. created a comprehensive 3D model for a DED process. The model looked at bead geometry

and input that into a FE model to predict mechanical and thermal effects from the process. The validated model allowed for residual stress to be reduced by varying parameters and geometry [32]. These tools are building blocks for reducing stresses, minimizing defects, and improving overall understanding of a complex process.

2.3. WIRE AM MELT POOL CONTROL

Process control is becoming a key thrust area for AM processes as they shift into production environments. One of the primary types of process control is melt pool control or otherwise termed laser power control. During a build, the part will retain a high amount of heat and the temperature will rise. Consequently, process parameters must be adjusted to keep the melt pool from getting too hot and causing defects.

Two of the most common types of control involve either melt pool temperature or melt pool size. Melt pool size and melt pool tail length are described by Figure 2.1.

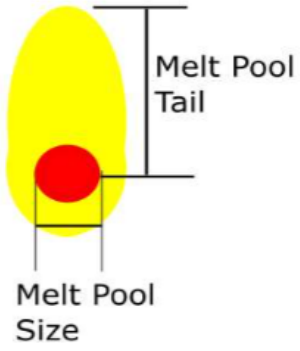

Figure 2.1. Melt pool measurement diagram

In a laser hot wire cladding process, a 2-channel pyrometer was implemented as feedback for a thermal control loop with the objectives of reducing dilution and maintaining a constant melt pool length. This work by Tyralla and Seefeld found a relationship between melt pool length and penetration depth and showed reduced dilution for both a stainless steel and a nickel alloy [30]. Though this method is effective for cladding on a cylindrical axis,

monitoring melt pool length can be more difficult with more complex motion. Kledwig et al. used the number of pixels (NOP) on a charge-coupled device (CCD) camera that were over a certain intensity to identify process instability in a DED process. In this context, instability, referred to deposition that would induce dilution or porosity problems [17]. This work helped improve process stability without being directional, but did not focus on overall heat accumulation in the build or geometrical concerns.

Gibson et al., explored different control methods based on melt pool size to both control energy input and bead geometry. The method with the best results combined using in-process laser power modulation as well as interlayer laser power scheduling. This allowed each layer to follow a closer estimation of input power with less change throughout. Additionally, it was able to account for areas of the build that would slow travel speed and normally cause material build up. This was highlighted by building an acute angle with and without control, with the in-control angle yielding a much more uniform result [12].

2.4. WIRE AM HEIGHT CONTROL

Height control methods for metal AM vary but can be broken into two main categories. The first being out-of-process and the second being in-process. In-process has two big advantages of reduced processing time and the ability to prevent deviations. Though without a completely in-control process, those deviations may still occur so a combination of the two is viable for reaching ideal build geometry and quality.

2.4.1. Out-Of-Process. Of the former, a common technique involves using a scanner between layers, so that the part can be re-sliced or the process variables can be pre-planned to adjust through the path and correct. Li et al. proposed a solution of interlayer scanning and adjusting parameters of the next layer for correction. The results were effective at controlling the height for most situations. However, the authors note that the adjustments to parameters could still be wrong due to error accumulation and would not control bead width. They combat this challenge by keeping track of the scanned layers for

the model rather than just looking at the previous layer [19]. Garmendia et al. focused on more complex geometry using an approach that featured structured light scanning. This technique kept the scanner in one position to remove any induced error from the motion itself which could be confounded with the height measurement. After scanning, the part could either be continued, or the path could be regenerated if the deviation was too great. The number of layers could then be changed so that the final part would match the CAD model as closely as possible. The results were promising in achieving the correct geometry and reducing post process machining [10]. In a WAAM process, current was used as a feedback mechanism for stick-out. Stick-out in this process is the distance from the weld contact tip to the workpiece. The average measured current of a layer was used as an input to an interlayer function. Between layers, z height was adjusted to maintain a stick-out that would result in a stable process. Scetinec et al. used this re-slicing feedback loop to not only keep the process stable, but also build to correct geometry [24].

2.4.2. In-Process. Takushima et al. looked at previous layers in front of the deposition with a line beam. To get a useful scan, a band pass filter of the line beams wavelength was placed to block the intense light from the melt pool and pass the beams wavelength. The scan approximated the bead height and width which could then be used to estimate the wire feed speed necessary to correct the height throughout the layer. This method was evaluated by building cylindrical walls with different commanded layer heights and measuring the gap between the nozzle and workpiece. The results showed how the control method allowed the build to be completed even with incorrect layer heights that would normally cause stubbing or droplet formation [29]. Work done by Hagqvist et al. proposed electrical resistance measurement as a method for control of a hot wire LMD-w process. Using this method, they were able to adjust the stick-out distance between the robot and melt pool to maintain process stability [14]. Too long of a stick-out distance can cause droplet formation and too short of a stick-out can cause the wire to bend and stub. Both of these potential defect causing scenarios are demonstrated in Figure 2.2.

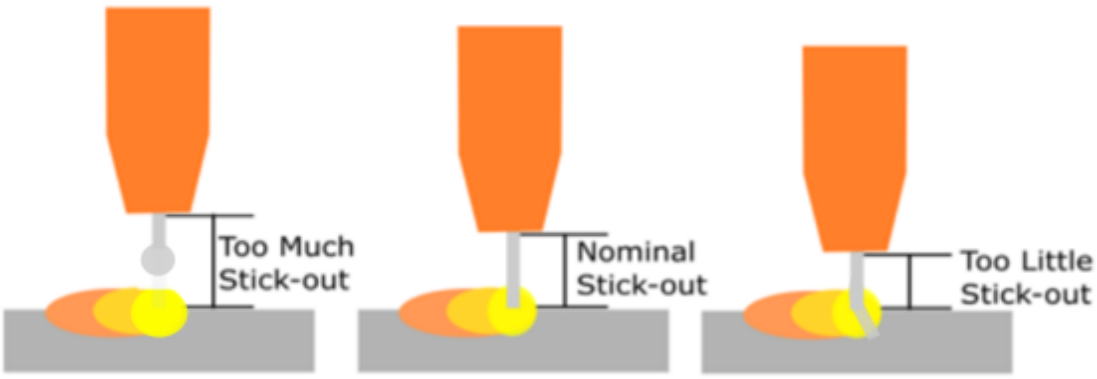

Figure 2.2. Instability from incorrect levels of stick-out

Following work showed the method can be used on a cold wire system by adding in a wheatstone bridge, allowing implementation without major hardware or process changes. This work showed the method improved the deposition stability in thin walls, allowing them to be built higher without failure [13].

In summary, the laser hot wire DED process offers potential improvements in deposition rate, reduction in residual stress, and microstructure control. Numerical modeling can be utilized to better understand how the process parameters effect bead geometry. After understanding those effects, process control techniques can be implemented to further the technology.

3. MODELING BEAD GEOMETRY

This section will discuss the formation of a mathematical model that describes the input parameters laser power, travel speed, deposition rate, and hot wire power, and how they influence bead geometry. This will be described by measurements that capture both the overall height/width and the shape of the bead.

To better understand how inputs in the laser hot wire system effect bead geometry, a mathematical model was formed and fitted to results from a 4 factor experiment. Analytical models of similar processes have been formulated with outputs of bead height, width, area and sometimes wetting angle [31],[4], [3]. Area, height, and width are the most obvious and provide most of the information. However, using just those can miss crucial information about the shape of the bead. The cross sectional area of the bead as well as how it is distributed are important for any type of weld, especially in AM where beads will be stacked both side by side and on top of one another. Models with wetting angle tend to more accurately predict the overall shape of the bead. The model in this work seeks to more completely capture the bead geometry by using both area and another term, full width at half maximum (FWHM), to describe the bead. A visual representation of these measurements is shown in Figure 3.1.

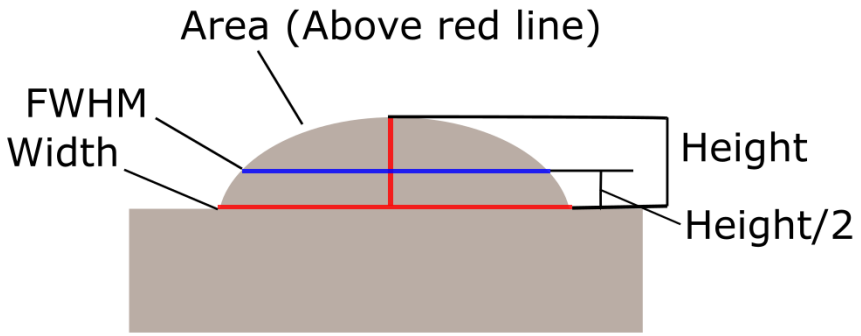

Figure 3.1. Bead measurements found with image processing

This is because even with a favorable wetting angle, a bead can still be low in the center, resulting in unfavorable geometry. The form of the model is described in Equation 3.1.

$$\begin{bmatrix} Height \\ Width \\ Area \\ FWHM \end{bmatrix} = f(LP, TS, DR, HW) \tag{3.1}$$

The data used for this model was collected from an experiment that consisted of 2.5 inch long deposited beads each with a different variation of all of the 4 parameters. Due to the proprietary nature of the experiment no other details of the experiment can be released.

The plates were then cut in half to reveal the cross section of the bead. These cuts were place in the middle of the bead, to avoid introducing error from start and stop conditions of the deposit. The beads were then imaged, shown in Figure 3.2 at a consistent magnification and stored for later computations.

3.1. IMAGE PROCESSING

To streamline the data collection and analysis, Python programming was used. With the black background used in the photos, a binary dilation was able to differentiate the background from the titanium. This new binary image could then be used to trace the outline of the material as shown in Figure 3.3.

Due to the imaging setup, some of the plates were not completely square, so the border of the material was identified as the substrate level. The image was re-scaled from pixels to mm based on the magnification of the microscope. The image was then fitted into an xy coordinate system that could be used for further analysis without interpolating for each calculation. Figures 3.4-3.5 show the next steps, breaking the bead into sections

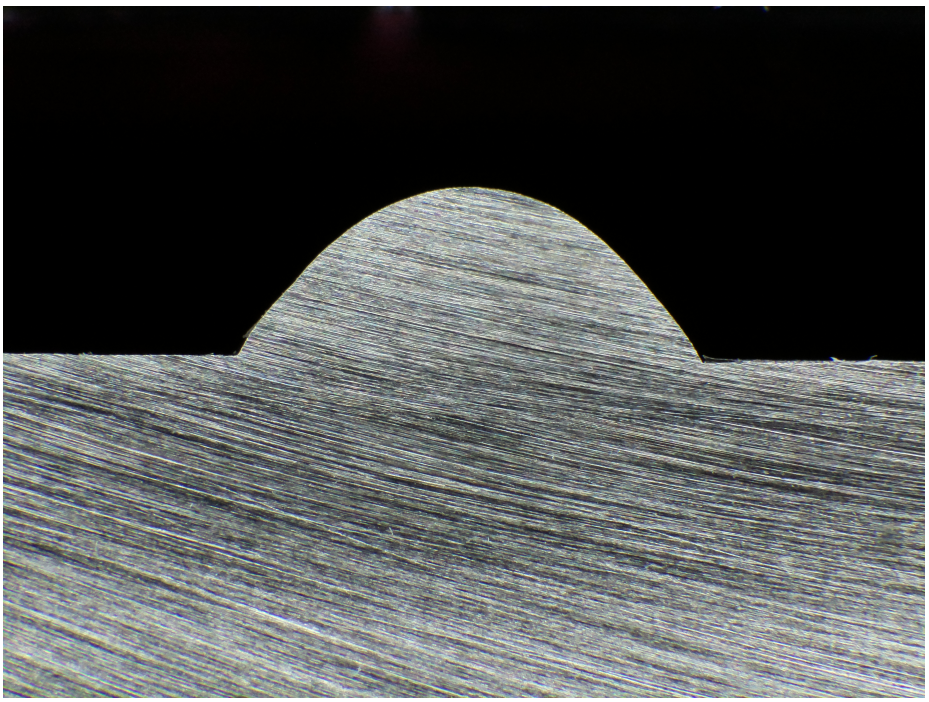

Figure 3.2. Raw cross section of bead optically imaged

in both directions for calculating measurements. The overall height and width were found from the longest section in the vertical split and horizontal split, respectively. The area was calculated as the sum of the sections. The FWHM was found by finding the length of the horizontal section at half the height of the full bead.

The image processing code took in 152 images from a folder and returned a numpy array. Each row in the array represented an experimental run with input parameters and resulting measurements. This array was stored for model fitting.

3.2. MODEL FIT

This section will describe how the from of the model was chosen and then how it was fit to the experimental data. In a hot wire GTAW process, Kannan, Muthupandi and Devakumaran focused on the heat input into the process, both to melt substrate and filler material [16]. The main energy input into the process was mainly driven by welding

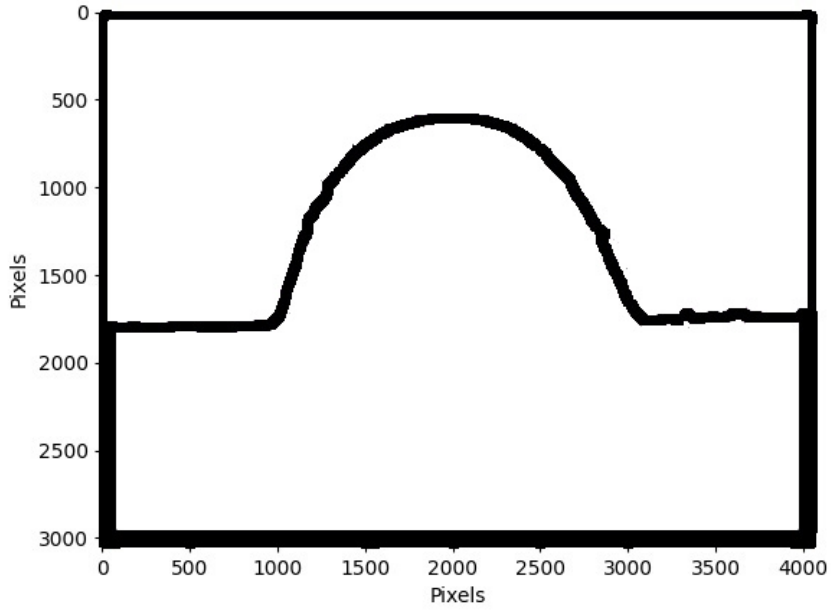

Figure 3.3. Material border capture

voltage,current, and travel speed. They additionally added a separate component for the hot wire aspect of the process defined as the power input over the wire feed rate for the preheating. These inputs were used to look at bead width, area of base material, area of filler metal and dilution. In this context and the context of this paper, dilution is defined as the area of the parent metal melted to the total area of the melt. This allowed the researchers to gain a better understanding of the process and tailor parameters to a better bead shape [16]. Similarly, the DED process is driven by the energy input into the material as well as the total material melted. For this process, the energy input is defined as the laser power (LP) and the hot wire power (HW) input into the process. The total material melted consists of the wire deposition rate (DR) and the portion of substrate or material re-melted known as dilution. This is shown as travel speed (TS) in the equation. The driving equation for DED is known as energy density (ED) [33]. The form of the equation is modified to include heat input from the wire preheat and the chosen form is described in Equation 3.2.

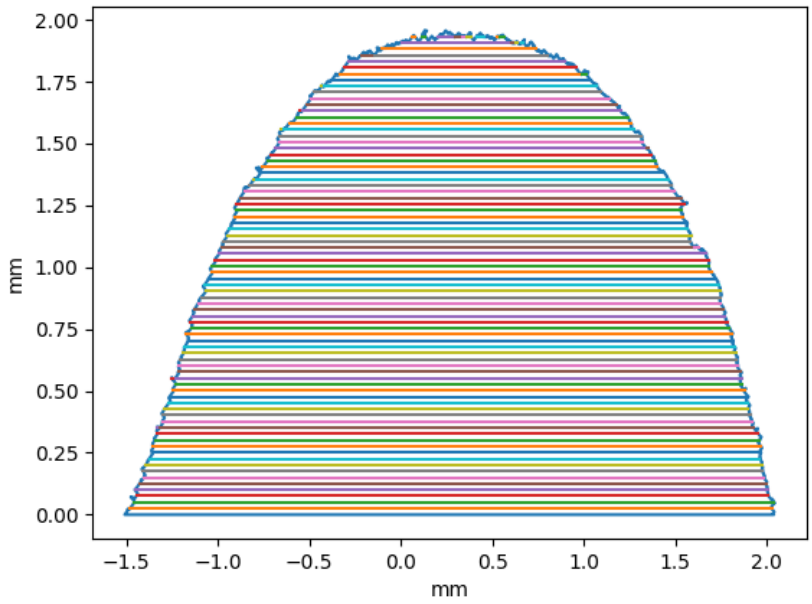

Figure 3.4. Horizontally split bead cross section

$$ED = \frac{LP + HW}{TS * DR * SS} \quad \left[\frac{J}{kg/hr * mm^3}\right] \tag{3.2}$$

Since each aspect measured is affected differently by energy density, coefficients were fitted for each separately. These coefficients not only fit parameters for different measurements, but also include error terms that are difficult to capture individually. These include things like laser power loss due to reflection, material vaporized, energy loss into the substrate and energy losses in the preheating loop for the hot wire system. Since spot size is fixed, the coefficient is set to 1. For simplicity, it is removed from the computations and the resulting general form for the fit model is then Equation 3.3

$$ED = \frac{LP^a + HW^b}{TS^c * DR^d} \tag{3.3}$$

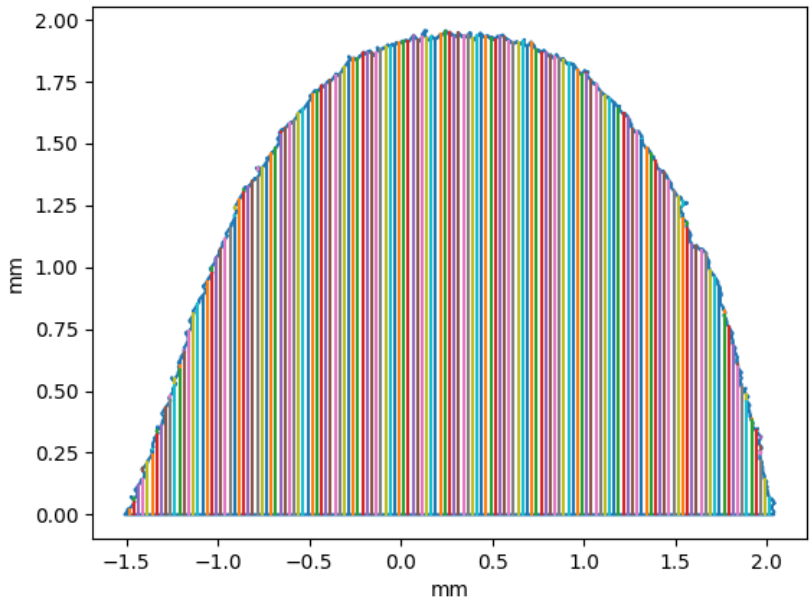

Figure 3.5. Vertically split bead cross section

After finding the form of the equation, the previous data generated in Section 3.1 was used to fit the coefficients. Python programming was utilized to do the fit. A function was defined for each measurement with the general form described in Equation 3.3. Each was coupled with a function that took estimated coefficients and experimental data as inputs. This function returned the error between the model fit and the experimental run and will be referred to as the error function. The error function was then available in a form to be fit with model fitting tools. The optimize.minimize function from the Python library Scipy, took in the error function and the coefficients specified as inputs. The minimize function iterated through the data set to find the lowest value for the error function. This resulted in the lowest error between the model and experimental data. Using this tool, Equations 3.4-3.7 were fit to the data set.

$$Height = \frac{LP^{0.282} + HW^{-0.550}}{TS^{0.387} * DR^{1.005}} \tag{3.4}$$

$$Width = \frac{LP^{0.208} + HW^{-0.021}}{TS^{-2.342} * DR^{0.156}} \tag{3.5}$$

$$Area = \frac{LP^{0.541} + HW^{-0.69}}{TS^{0.563} * DR^{1.313}} \tag{3.6}$$

$$FWHM = \frac{LP^{0.219} + HW^{-0.154}}{TS^{0.015} * DR^{0.331}} \tag{3.7}$$

After the fit was performed, 15 data points that were reserved were now used to verify the model. The results were described by the sum of squares error (SSE) and both were satisfactory as shown in Table 3.1.

Table 3.1. Model Error Results

Measurement Type	Data SSE	Check SSE	Data Avg. Error	Checkpoint Error
Height (mm)	0.123	0.014	0.030	0.030
Width (mm)	0.233	0.034	0.048	0.041
Area (mm^2)	0.320	0.051	0.058	0.048
FWHM (mm)	0.120	0.014	0.030	0.030

These numbers reflect predictions being within 120 microns of each measurement, a change which can be seen along the length of a bead that is not fully stable. These results show not only that the model is a good fit, but also that the data set used had enough points to approach a stable amount of error.

4. METHODOLOGY

To perform the experiments, a 500A Miller Laser Hot Wire System, a 4kW Laserline diode laser, a Fraunhofer COAXWire deposition head and a delta parallel robot were integrated. This was achieved using LinuxCNC, an open-source machine control software along with a field programmable gate array (FPGA) card. The FPGA controls the servo drives according to an inverse kinematics model in LinuxCNC allowing the center of the robot to translate in 3 axes while maintaining the orientation of the end effector. Additionally, the FPGA provides both digital and analog IO that were utilized for the integration of the subsystems. The deposition system is pictured in Figure 4.1.

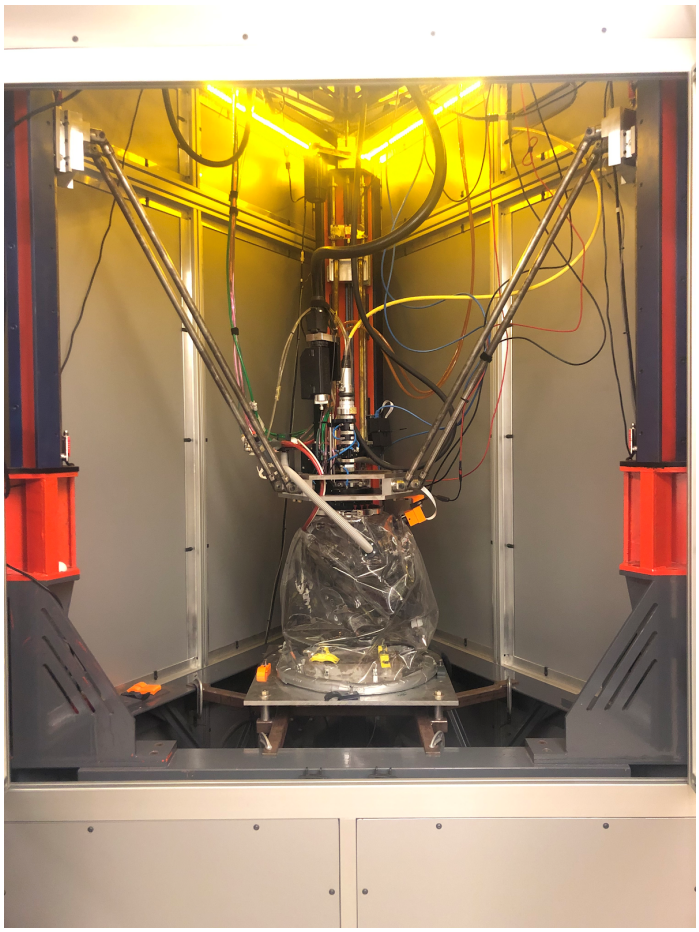

Figure 4.1. Integrated Deposition Cell

4.1. PARAMETER SPACE EXPLORATION

Deposition attempts were performed to find a baseline for stable process parameters. Due to the complexity of the process, these first attempts had stability issues. To improve this, parameters were varied across a wide range to find a stable set. Figure 4.2 shows theses attempts and some of the droplet formation from improper parameters. The tracks deposited were 3 inches long and spaced 0.25 inches apart.

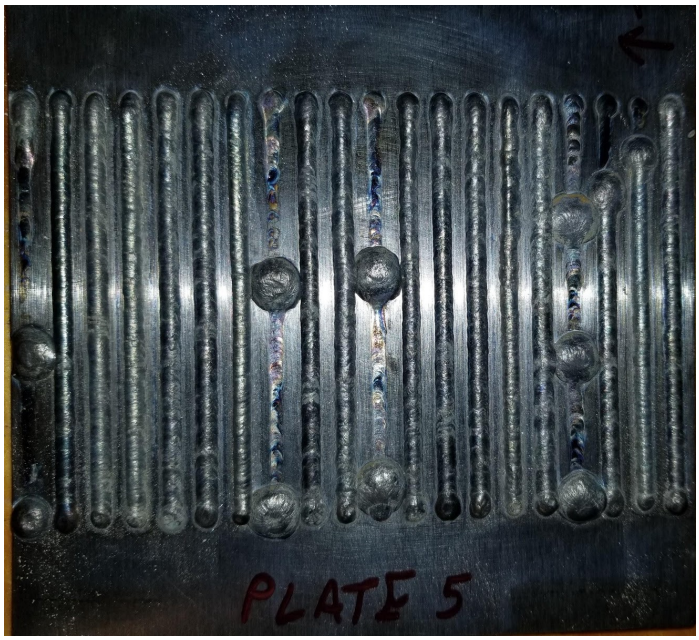

Figure 4.2. Plate from initial parameter exploration

Droplet formation occurs when there is not enough wire being input for a given parameter set. On the other end of the process window, too much wire input can cause stubbing and surface defects. Sometimes this stubbing can cause the wire to leave the melt pool entirely, though with the coaxial wire delivery, this is less common. Surface defects caused by stubbing are shown in Figure 4.3.

Figure 4.3. Surface defects due to stubbing

4.1.1. Oxidation. Early Ti-6Al-4V deposits from this cell were oxidized and had clear discoloration. This titanium alloy will form an oxide layer when any oxygen is in the atmosphere at temperatures above 400°C [6]. An inert environment was added to the system to reduce oxidation. The improvement was effective as shown in Figure 4.4, so the inert environment was used for all deposition moving forward. Additionally, the oxidation has an impact on surface tension and therefore bead shape. Meaning it would prove difficult for height control.

Figure 4.4. Deposition with and without an inert environment

4.1.2. Stepover Concerns With High Deposition Rates. After the initial parameter exploration with hot wire deposition, it became a concern that its taller bead geometry may make achieving fully dense deposition difficult. Figure 4.5 shows two beads with similar track width that have drastically different overall heights to demonstrate the difference.

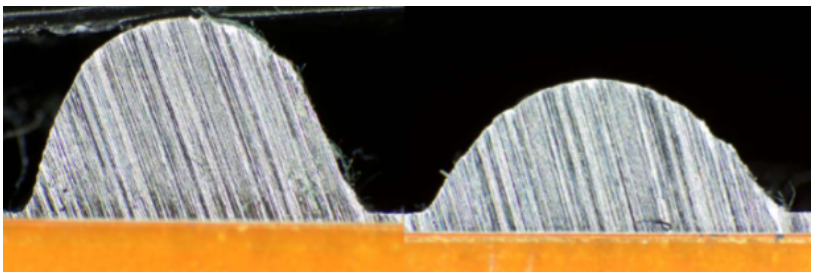

Figure 4.5. Cross section of beads with different wire feed rates

The taller bead, due to its peaky shape, makes stacking beads next to it more difficult. This can cause some of the laser energy to be blocked by the material from the initial track. The remaining energy may not fully melt the material in the subsequent tracks, inducing lack of fusion (LOF) defects [25]. Due to this added complexity, the scope of this work did not investigate builds with more than single bead walls.

4.2. PROCESS CONTROL ARCHITECTURE

As the process became more mature, the need arose for process control. Due to the wide range of potential control methods it was necessary to setup the architecture to be flexible and accept different types of feedback with different communication methods. The designed architecture is shown in Figure 4.6.

It allows not only feedback sensors, but also communication between other tools such as simulations and CAD/CAM software. This architecture allows the deposition controller to maintain timing, which is crucial for stability in the deposition process. The deposition controller then communicates with the on-demand control module as needed. This can be on a timed basis or on an event basis, depending on the function. The on-demand control module can then perform more time consuming or computationally demanding tasks without disrupting the process. This allows flexibility to add onto the system without sacrificing performance.

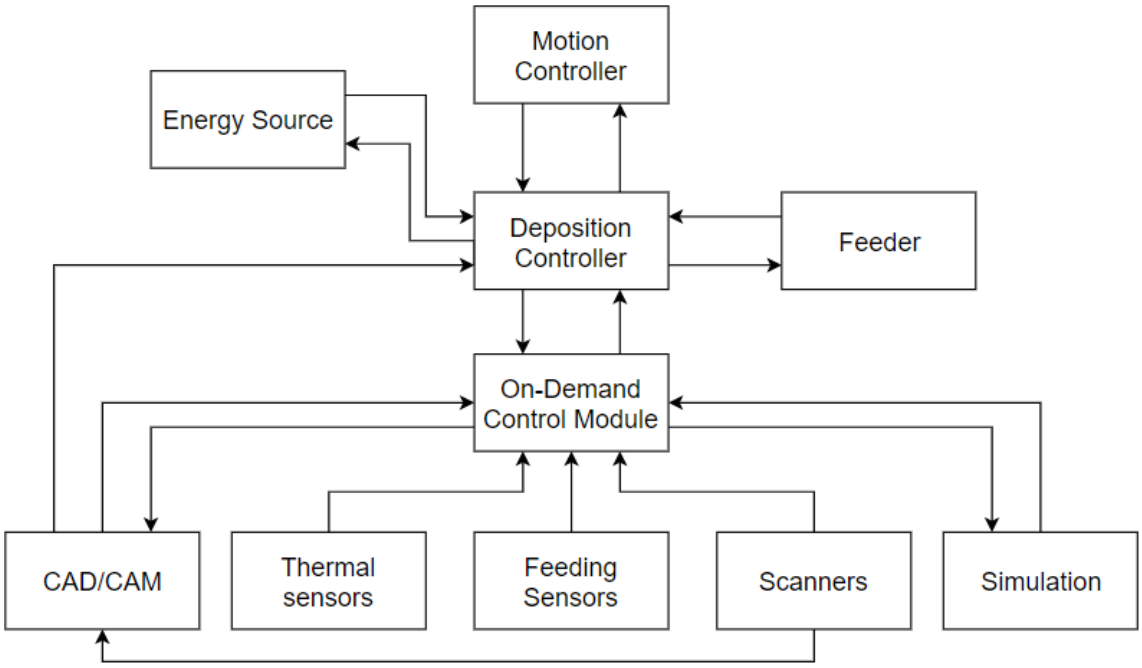

Figure 4.6. Process control architecture

4.3. LASER HOT WIRE

4.3.1. Electrode Extension Control. The Miller Laser Hot Wire system used in this work is controlled based on maintaining a constant enthalpy in the input wire. Equation 4.1 is the governing equation for this principle with the left side containing electrode extension shown as EE, wire enthalpy represented by λ, and I as current. On the right are constants of wire diameter, D_w, and the density of the electrode material,ρ_w. The other variables in this equation are wire feed speed, shown as τ, and $H_f - H_o$ represent the desired change in enthalpy from ambient conditions [26].

$$EE * \lambda * I^2 = \left[\frac{\pi D_w^2}{4}\tau\rho_w\right][H_f - H_o] \tag{4.1}$$

Equation 4.2 rearranges the previous equation to show current, I, is proportional to the change in electrode extension [26]. Thus, making it a viable option for feedback in a control system. Scott et al. leveraged this to patent a control method for regulating electrode extension in a robotic welding process by moving the end effector closer or farther from the workpiece [26].

$$EE = \frac{\pi D_w^2 \tau \rho_w (H_f - H_o)}{4\lambda I^2} \tag{4.2}$$

While this method can be effective for electrode extension, the same principle can be applied to wire fed AM. In this work, the constant enthalpy system on the Miller welder provides current feedback that similarly can be used to measure the height of the deposition. The corrective action investigated in this work modulates travel speed of the motion system to control deposition height rather than regulate electrode extension.

4.3.2. Bead Height Control. This work uses the previous logic for a different application. Since it was established that the electrode extension is proportional to the weld current, that measurement needed to be taken and understood. This system measures the voltage drop from before and after the process. For this voltage drop, there is a resistive circuit that consists of the wire from the first measurement point to the workpiece and the workpiece to the second measurement point. Most of this is fixed, so the electrode extension is assumed to be the main source of variability in the circuit. Due to that, Ohm's Law can be used to calculate current for a given electrode extension. The diagram in Figure 4.7 shows the setup described.

Since the distance from the weld contact tip to the workpiece is fixed, the electrode extension length plus the height of the bead is fixed. Therefore, for a specific electrode extension, a height can be estimated. With this understanding, bead height can be controlled using current feedback.

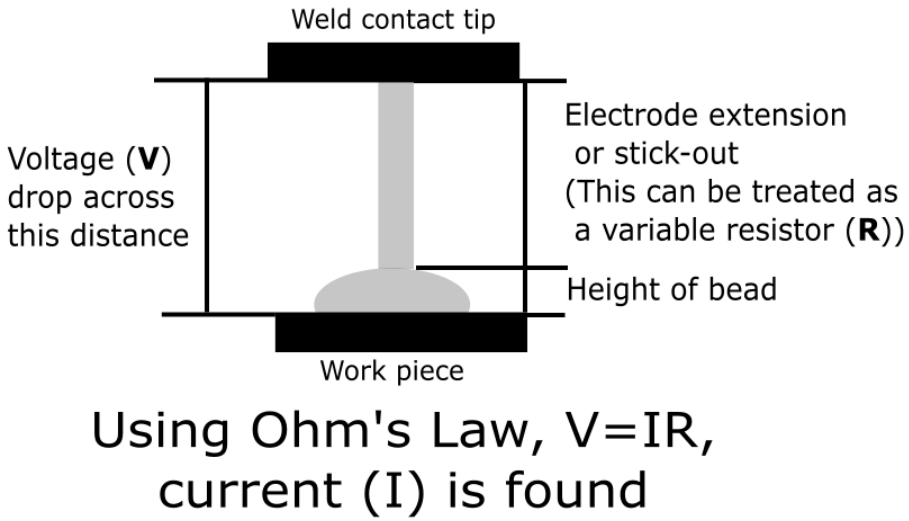

Figure 4.7. Current output at different levels of stick-out

4.4. CURRENT FEEDBACK MEASUREMENTS FOR SPC

Before implementing the height control method, verification of the system's capability to measure bead height needed to be established. Data was collected in an attempt to develop statistical process control (SPC) of the height of the deposition process.

To measure large changes in bead height, an exaggerated case was used to gather data. This involved depositing on plates that had high and low spots of a known height and depth, respectively. The low spots were induced by milling 1 inch wide slots into the center of the substrate perpendicular to the deposition direction at a depth of 40 thousandths. The high spots were induced by milling 1 inch wide slots on the outside of the substrate perpendicular to the deposition direction at a depth of 40 thousandths of an inch, then using the lower depth as deposition height. This setup more accurately simulated missing material or buildup that would occur during normal operation. Data was collected for each of the three cases with three repetitions, then averaged.

Figure 4.8 shows how the setup was capable of detecting low and high features using the current feedback from the welder. The spikes in the beginning are from the welder attempting to establish an "arc", once contact is made with the workpiece, it reduces to

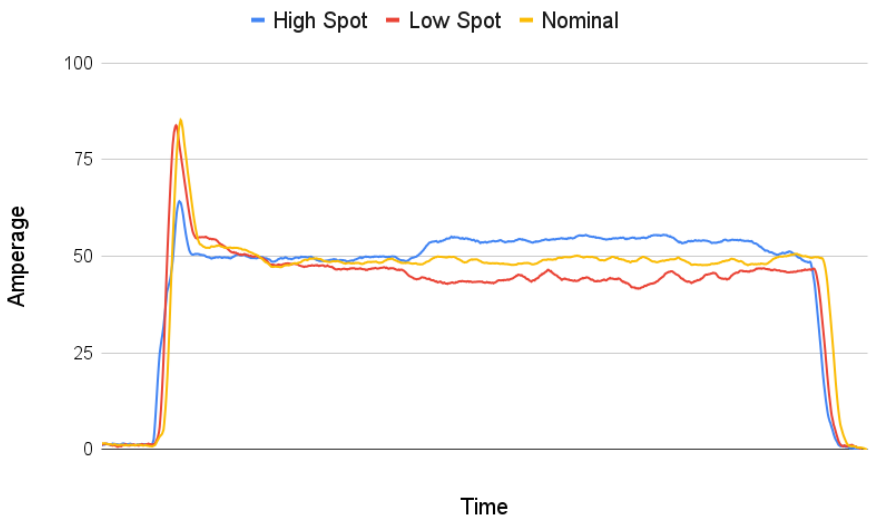

Figure 4.8. Current across induced low and high spots

steady state. For the nominal standoff, the amperage stay stable until the end of the deposit. When the deposition head is over a high spot, we see a jump in amperage. This is as expected, since the effective resistance is reduced from a shorter electrode extension. In the case of a low spot, we see a longer electrode extension and therefore a drop in amperage. With a measured amperage drop over a specific change in electrode extension, the control loop was able to be calibrated.

4.5. TRAVEL SPEED AS CONTROL VARIABLE

With the data collected, the feedback loop could now be added and tuned to control deposition height. For this work, the travel speed of the robot during deposition was used as the control variable. This is mainly to fully understand the control loop. Since deposition rate and hot wire input directly change the current feedback used for control, they are confounded. While this does not make the control loop impossible, it does make it much

more challenging to understand set points and variations. Since travel speed was chosen, when the controller detected a low spot, the robot would slow down in an attempt to fill in the missing material. For a high spot, the robot would speed up and lay down less material.

This control method was implemented in the architecture described in Section 4.2. In this case, the control module takes in the current feedback from the welder and uses a proportional–integral–derivative (PID) loop to return a value for the travel speed override to the deposition controller. A block diagram of the control loop is shown in Figure 4.9.

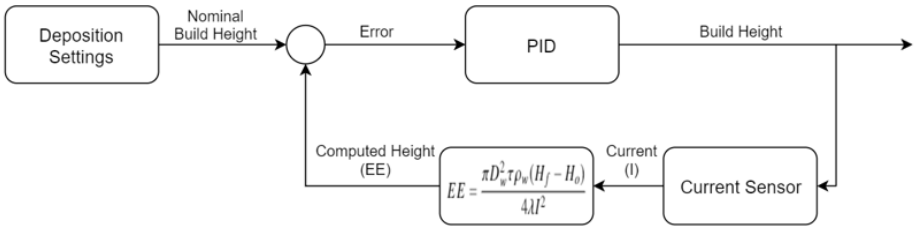

Figure 4.9. Height Control PID Loop Block Diagram

Initial PID tuning began by slowly increasing P gain. This had little effect on the process until the P gain was increased significantly. Eventually, the P gain was so high that the travel speed was too high or low and the process became unstable, causing droplet formation or stubbing. Once a stable range of speed override was found (P gain was tuned), the response time had to be tuned as well. In Figure 4.10, artifacts of quick back and forth responses are clear throughout the wall. At these points, the track gets wider and smaller again causing a "caterpillar" effect that is not sustainable for maintaining geometry throughout a build.

To mitigate this, two types of filters were considered; a finite impulse response (FIR) filter and a infinite impulse response (IIR) filter. Though the two are similar, an IIR filter uses previous outputs in its calculations. This keeps the changes in output closer together and smooths the response. Though smoothing is preferred, this would allow a spike such as those shown in Figure 4.8, to bias the response high for a longer period of time and sacrifice

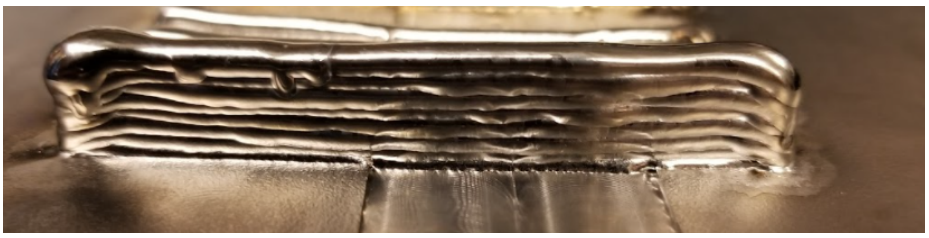

Figure 4.10. Thin wall with over-correction artifacts

accuracy. Due to this, the FIR filter stood a better chance of maintaining the balance. The filter essentially kept a moving mean of the data points collected and fed that value to the PID controller. This eliminated overreaction to momentary spikes in data and resulted in an overall smoother response. One limitation to filtering is that it may miss events or cause a delayed response. In AM height control, this would actually cause the controller to amplify the error and make the error even higher in the next layer. Thus, it is important to balance the number of samples in the filter to smooth the response without causing significant delays. A thin wall, Figure 4.11 was built on a plate with an induced high spot to show results of a balanced filter size.

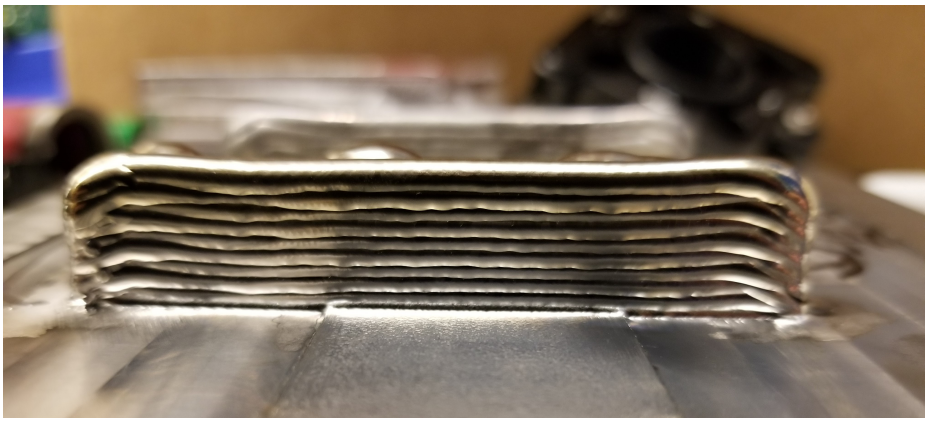

Figure 4.11. Thin wall made with FIR filter

While it is not completely smooth, it shows significant improvement and was used as a baseline for further development.

5. EXPERIMENTS

Thin walled structures are very common in literature since they are easily programmed and showcase process stability when built successfully. This is mainly due to start and stop behaviors of the deposition process. Without proper tuning, high spots show up at the start and the material slumps at the stops. This error propagates through the part and other variations in the build are accentuated by it. For those reasons, thin walled structures were chosen for height control investigation.

To test the efficacy of the height control method previously outline in Section 4.5, a small experiment was performed. A set of 3 thin walls was built for three different levels of control. The walls were built at 4, 8, and 12 layers tall for each level. This allowed the error in height to be quantified as it stacks up. The walls built with height control could then be evaluated against the baseline. The idea being that an in-control process would have an error of +/- an amount for each wall. In contrast, the error in an uncontrolled process would continue to increase with the number of layers. This would verify height control could correct for a certain amount of error in buildup. Another form of verification, and possibly more importantly, is the ability to even out the thin wall. With experimentation, generally a proper layer height can be found. However, depending on heat buildup and other factors, low and high spots can occur. Fixing those spots, as well as preventing them from getting worse, can be important to both completing a build and reaching near net shape geometry.

Results in Table 5.1 show the effects of adding height control and increasing the level of control on the process's ability to build flat. In this experiment, control level -1 is uncontrolled, 0 is a low level of control response and 1 is a high level of control response. An "(I)" indicates an uncompleted run due to process instability. Results showed that the higher response was the most effective at achieving layer flatness.

The same experiment was evaluated for overall error in height. The results are summarized in Table 5.2 and favored the middle level of control response.

Table 5.1. Height Control Flatness Experiment Results

Control Level	Number of Layers	Deviation in Height (inches)
-1	4	.008
0	4	.009
1	4	.001
-1	8	.025
0	8	.008
1	8	.002
-1	12	.023 (I)
0	12	.012
1	12	.005

Table 5.2. Height Control Height Error Experiment Results

Control Level	Number of Layers	Error in Height (inches)
-1	4	.029
0	4	.019
1	4	.015
-1	8	.040
0	8	.006
1	8	.019
-1	12	.050 (I)
0	12	.015
1	12	.017

These tables indicated that the higher control response level was effective in flattening the build, however it did not produce the lowest error in overall build height. This may be due to incorrect layer height, variability in the complex process, or the control loop may not be able to keep up with how large the changes are at a high response level. Therefore, more experimentation would give a better indication of what level of control would be most effective.

6. DISCUSSION

This sections begins with a discussion of where the model can be effective, where its limitations are and how it can be improved. Results of height control experiments are then analyzed and discussed. The section ends with comments about how else the model can be leveraged to improve process control and overall understanding of other thermal processes.

6.1. BEAD GEOMETRY MODEL RESULTS

The geometrical model appeared to be an effective predictor, according to the error found in checkpoints. To further understand to what degree it was effective, process capability was evaluated using SAS JMP for each measurement. Since the actual value range varied with different parameter sets, a percent difference was chosen to normalize the data set.

Each predictor was evaluated at specification limits of +/-15% at a confidence level of 95%. The two main metrics in these process capability charts are process capability index, Cpk, and process performance index, Ppk. Cpk is a term that indicates if the process can potentially meet specifications. Ppk is a performance indicator and indicates how well the process is staying within specifications. The process is considered capable at a Cpk or Ppk value greater than 1.00 and is generally considered in control at values above 1.33 [23].

The first, area, showed a Cpk value of 0.857 and was not capable for this specification range. However, Figure 6.1 shows that none of the data points were actually out of range. For that reason, there is a Ppk value over 1. Gathering more data may show that the prediction is always within that specification, or continue along the curve estimated for a normal distribution. The next predictor, width, was shown to be capable at a Cpk value of 1.148. Though the distribution, shown in Figure 6.2 had a similar width to the area plot, more data points fell closer to 0, making it more likely to fall within the limits. Additionally, the Ppk landed at 1.386 indicating it was performing in-control.

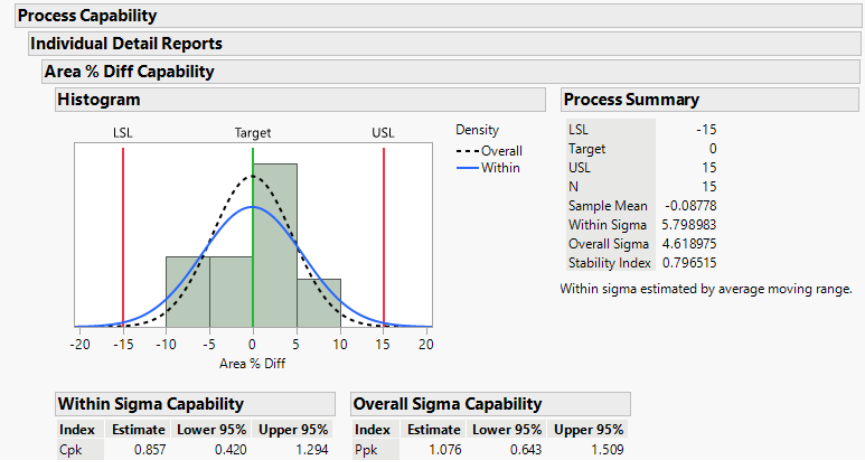

Figure 6.1. Area prediction capability

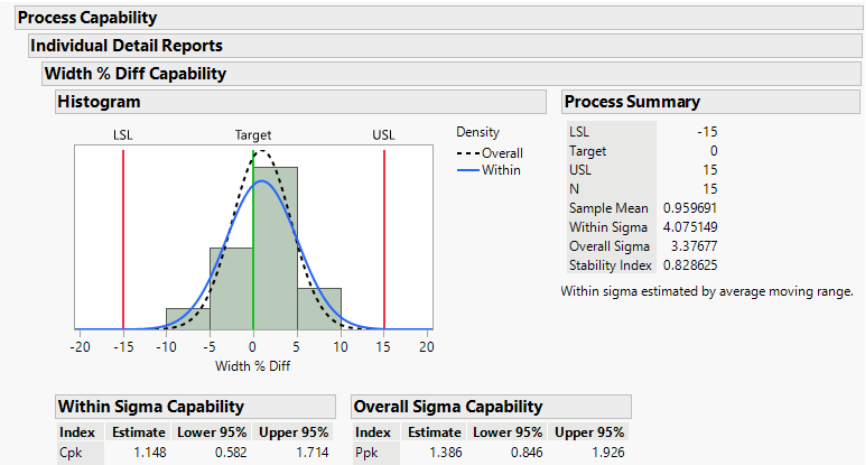

Figure 6.2. Width prediction capability

FWHM was barely capable at a Cpk of 1.052 and showed a distribution trending on the low side of the target in Figure 6.3. This is most likely due to the typical shape of a bead. Most of the area is distributed close to the substrate and there is generally a thin peak at the top. The Ppk for FWHM showed it to be capable but not in-control at 1.111.

The last predictor, height, showed the most promising capability with an in-control Cpk of 1.421. The Ppk value was slightly lower at 1.276 and not quite in-control. Figure 6.4, shows the tighter distribution of the height plot, trending slightly low.

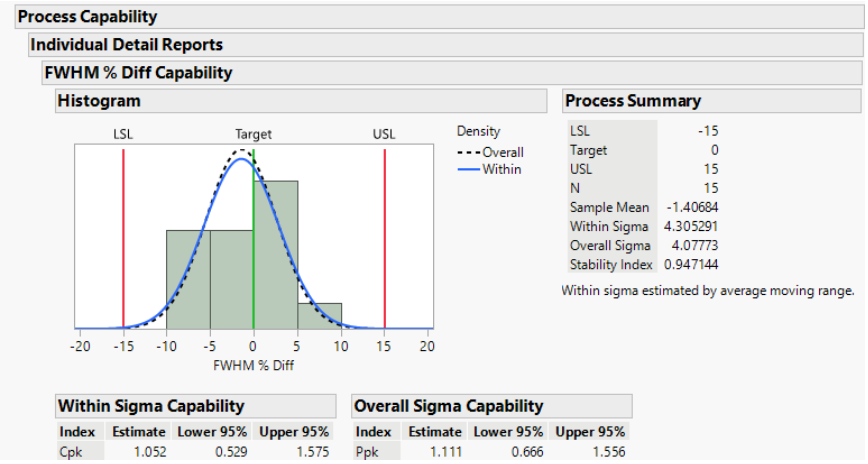

Figure 6.3. FWHM prediction capability

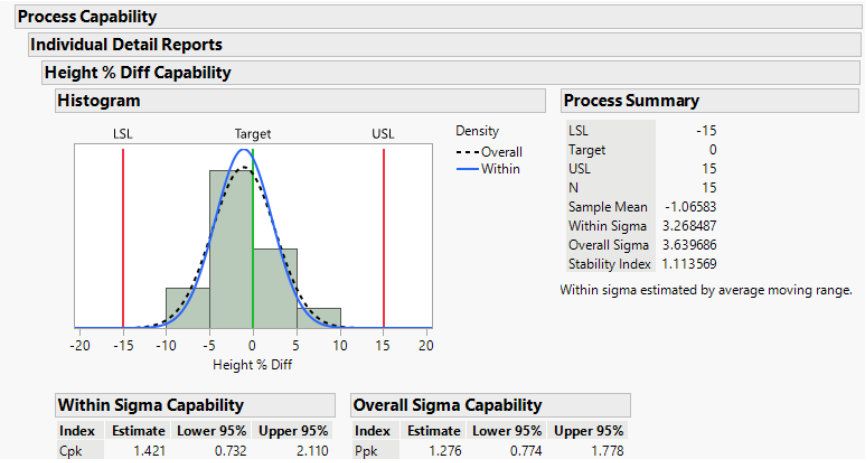

Figure 6.4. Height prediction capability

Generally, the height and width of the bead are most important when planning a build, since they will drive geometry. Due to that, it is crucial that the model is capable of predicting both of them within a reasonable percentage. These plots show that it was effective for a range of +/-15%, but there is room for improvement.

In this work, the model was used to understand how the geometry reacted to changes in certain parameters. Additionally how sensitive width and height were to different parameter changes. So for this application, the specification level was appropriate. However, when trying to fine tune process outputs, tighter specification limits may be necessary. In

that case, the tools presented can be applied to a larger data set. One limitation of this data, is that it was gathered from a single cross section for each bead. A full scan of the bead profile across the length of the bead may provide more insight on the consistency of the bead. If the process is not very consistent, these tools may not be able to predict precise values, and the trends presented may be the most telling.

6.2. EFFECTS OF PARAMETERS ACCORDING TO MODEL

With the model fit and proven to be capable of predicting bead geometry, it could be leveraged to better understand the process and how parameters affect the final bead geometry. Though many avenues can be taken to investigate bead geometry, this work focused on controlling the height of the bead to improve process stability. The goal here is to have the authority to change the bead height without large changes in the bead width.

The first bead prediction investigated was height. Travel speed, laser power, and deposition rate were compared in a range slightly over the experimental parameters. Figure 6.5 shows the gradient between the input factors.

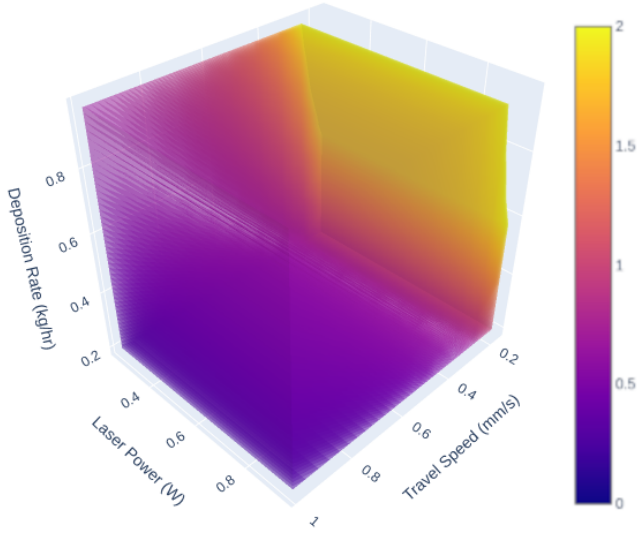

Figure 6.5. Parameter influence on height (colorscale in mm)

It is clear that the travel speed had the highest gradient, varying across the output scale. Though each factor did have an impact on the overall height. This is an expected result, as more material would be put in the same area and would stack up. More wire input, or deposition rate, would also increase the height, however with a higher travel speed it may not be appreciable. Laser power also would have little effect since it would control the temperature of the melt, not the material input. It would change the size and viscosity of the melt, so it cannot be ignored.

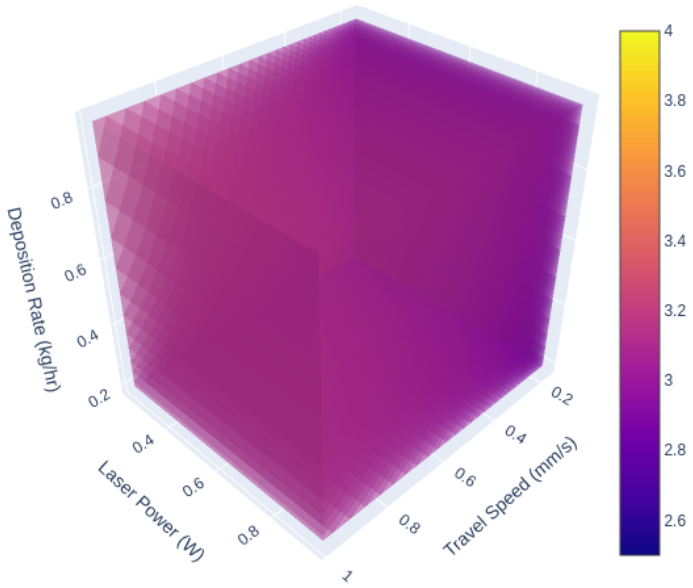

Figure 6.6. Parameter influence on width (colorscale in mm)

Width was then examined with the same input parameters so that a better understanding of the input-output relationship could be achieved. The width had a much more even gradient between factors, as shown in Figure 6.6. This meant that any of the methods would have a similar change in width, though travel speed seemed to still be the leading factor. Here we would expect that, as well as a low impact from deposition rate. The laser power effects seem to be just as significant as travel speed. Since these two are directly

impacting melt pool temperature and size, this result is as anticipated. The results of these predicted effects plots as well as other factors discussed in Section 4.5, justify the use of travel speed as a height control method.

6.3. HEIGHT CONTROL EXPERIMENTS

Regression analysis was performed for each experiment, to better understand the results. Each was performed at confidence level of 95% or significance value of $\alpha = 0.05$. Reviewing the experiment that looked at flatness of the top layer of a thin wall revealed that control level had a significant impact on flatness, with a p-value of 0.0375. From Figure

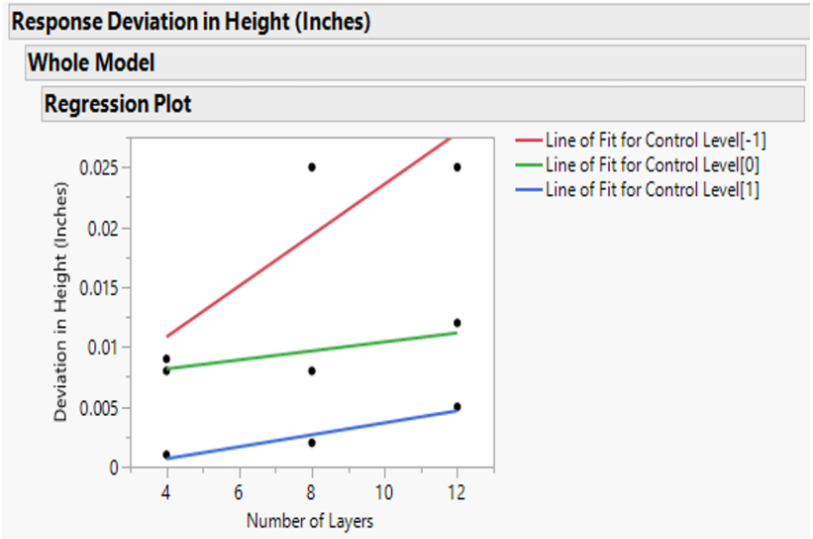

Effect Tests

Source	Nparm	DF	Sum of Squares	F Ratio	Prob > F
Control Level	2	2	0.00042022	11.8931	0.0375*
Number of Layers	1	1	0.00009600	5.4340	0.1020
Control Level*Number of Layers	2	2	0.00006100	1.7264	0.3170

Figure 6.7. Flatness experiment regression

6.7 we can see that higher control levels improve flatness, but there seems to be a trend with increased layer height as well. For an in-control process, we would expect the error to be

consistent throughout the build and not trend upward. Though the number of layers was not shown to be significant in this analysis, it is of note and may change with any additional data included in the study.

The overall height error of the build was also stabilized with control level. Figure 6.8 shows a p-value of 0.017, indicating control level effects were significant. For this experiment, the overall height error was driven towards zero with increased control.

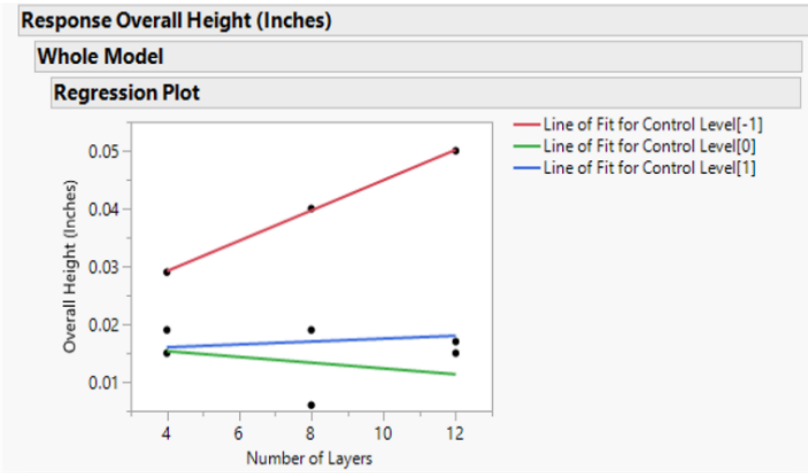

Effect Tests

Source	Nparm	DF	Sum of Squares	F Ratio	Prob > F
Control Level	2	2	0.00122067	21.0864	0.0171*
Number of Layers	1	1	0.00006017	2.0787	0.2450
Control Level*Number of Layers	2	2	0.00017033	2.9424	0.1962

Figure 6.8. Overall height experiment regression

The results of these experiments show the feasibility of the control method used in this work as well as areas that can be improved and trends that are of interest. Further demonstrations were performed to highlight use cases of height control.

6.4. CASE STUDY: XZ SLICED GOMETRY

While most of this work looks at slicing in the XY plane, the ability to control the height of the build opens up another possibility. If the control system is capable of maintaining the stick-out as the Z value increases, variable buildup can be achieved. Figure

6.9 shows a wall built with the robot moving up as it travelled across the build plate. This would normally result in the process becoming unstable since the stick-out would increase too much. However, with the control loop in place, the travel speed is adjusted to regulate build rate and maintain a stable process. This results in a complete build that imitates the toolpath.

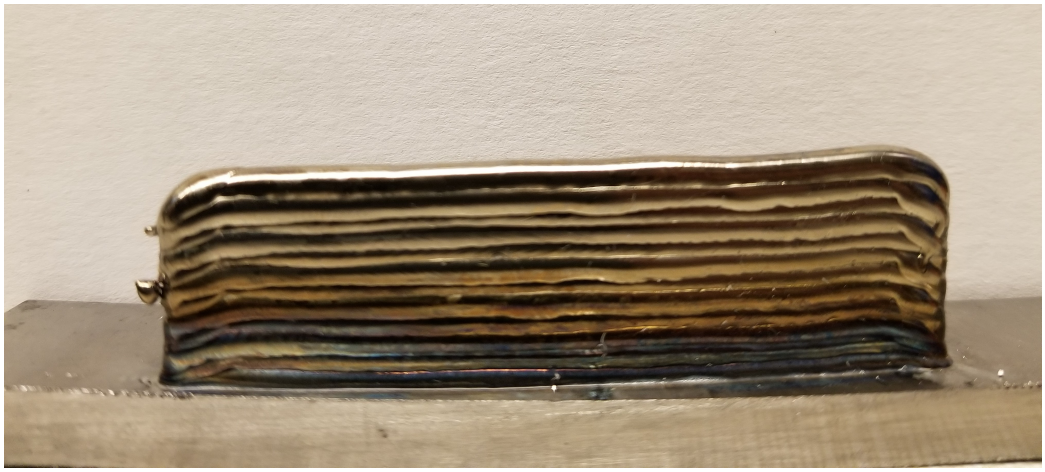

Figure 6.9. Wall built with increasing height across each layer

The gradient is increased each layer until for the last layer, the right side of the part is actually built up more than an entire layer height higher than the left side. Of course, this does not come without consequences. As shown by the effects plots in Section 6.1, changing travel speed will affect the width of the bead. In Figure 6.9, as well as other walls built with height control, there are clear artifacts from the melt pool changing size due to the travel speed of the motion system. The wall in Figure 6.9, was also attempted without height control, but was stopped after 5 layers due to excessive stubbing. Three trials were performed with and without height control, and the results were the same for each case. While this does not prove the height control is the reason for the build's success, it is a strong indicator. The walls were further examined to understand the outcomes. The stubbing from non height controlled walls was obvious from the process camera, but a cross section revealed more detail. Figure 6.10a shows that some of the material actually stubbed

out of the melt pool, leaving pointed artifacts on the top two layers. The controlled wall in Figure 6.10b had more consistent geometry and no stubbing artifacts, though some changes in width are observed.

(a) Wall without height control (b) Wall with height control

Figure 6.10. XZ Plane Wall Cross Sections

This case shows one potential application where having process control can actually provide improved capabilities. An in-depth understanding of the key process variables and how they influence bead geometry in a three dimensional space paired with strong process control opens opportunities for slicing in different planes as well as non-planar geometries.

6.5. FURTHER APPLICATION

As discussed in 2.3, laser power control is a common method of process control for this kind of process. This work presents a model that can be used as a tool to predict how geometry will change with any parameter change. Laser power control can be combined with height control to balance out unwanted changes caused by the other control method. With one process driving and the other supporting, both heat input and geometry control could be achieved.

However this tool is not limited to laser hot wire DED with titanium or even DED overall. The driving equation for the model is based on heat input for a unit of volume. Many other processes are driven by heat input and the methods presented can be used to gain a better understanding of those processes.

7. CONCLUSION

This work focused on understanding how an additional process variable, hot wire preheating, adds to the complexity of a typical DED process. The following conclusions highlight how the input parameters affect the output bead geometry and how travel speed can be used to drive control of the bead height in DED builds.

An analytical model based on energy density that included hot wire preheating was used to predict bead geometry from the deposition process. Process capability studies showed that the model was capable of predicting height and width of the bead within +/- 15% across a wide range of parameters. The model predictions indicate that travel speed is a good candidate for process control since it has high authority on bead height with limited effect on bead width.

The proposed height control method, utilized with the hot wire system, was shown to reduce the deviation in height along the length of the bead by over 200%. Additionally, overall build height error was reduced and trended toward 0 in thin wall builds. A case study showed that the control method could be expanded to compensate for under and over building in parts sliced in the xz plane rather than the xy plane.

REFERENCES

[1] URL: https://www.nist.gov/system/files/documents/el/isd/NISTAdd_Mfg_Report_FINAL-2.pdf.

[2] URL: https://www.sae.org/standards/content/ams4999/.

[3] M. Ansari, R. Shoja Razavi, and M. Barekat. "An empirical-statistical model for coaxial laser cladding of NiCrAlY powder on Inconel 738 superalloy." In: *Optics & Laser Technology* 86 (2016), pp. 136–144. DOI: 10.1016/j.optlastec.2016.06.014.

[4] M. Ansari et al. "A mathematical model of laser directed energy deposition for process mapping and geometry prediction of Ti-5553 single-tracks." In: *Materialia* 12 (2020), p. 100710. DOI: 10.1016/j.mtla.2020.100710.

[5] Markus Bambach et al. "Comparison of laser metal deposition of Inconel 718 from powder, hot and cold wire." In: *Procedia CIRP* 74 (2018), pp. 206–209. DOI: 10.1016/j.procir.2018.08.095.

[6] Rodney Boyer. *Materials properties handbook: titanium alloys*. ASM Internat., 1998.

[7] E. Brandl et al. "Additive manufactured Ti-6Al-4V using welding wire: comparison of laser and arc beam deposition and evaluation with respect to aerospace material specifications." In: *Physics Procedia* 5 (2010), pp. 595–606. DOI: 10.1016/j.phpro.2010.08.087.

[8] *Directed Energy Deposition (DED)*. June 2019. URL: https://www.digitalalloys.com/blog/directed-energy-deposition/.

[9] J R Fessler et al. "1996 International Solid Freeform Fabrication Symposium." In: URL: http://hdl.handle.net/2152/69928.

[10] Iker Garmendia et al. "Structured light-based height control for laser metal deposition." en. In: *Journal of Manufacturing Processes* 42 (June 2019), pp. 20–27. ISSN: 15266125. DOI: 10.1016/j.jmapro.2019.04.018. URL: https://linkinghub.elsevier.com/retrieve/pii/S1526612518306030 (visited on 06/29/2021).

[11] A. Germain et al. "An innovative method to assess and manage residual stresses in additively manufactured titanium." en. In: *MATEC Web of Conferences* 321 (2020). Ed. by P. Villechaise et al., p. 03030. ISSN: 2261-236X. DOI: 10.1051/matecconf/202032103030. URL: https://www.matec-conferences.org/10.1051/matecconf/202032103030 (visited on 06/01/2021).

[12] B.t. Gibson et al. "Melt pool size control through multiple closed-loop modalities in laser-wire directed energy deposition of Ti-6Al-4V." In: *Additive Manufacturing* 32 (2020), p. 100993. DOI: 10.1016/j.addma.2019.100993.

[13] Petter Hagqvist et al. “Resistance based iterative learning control of additive manufacturing with wire.” In: *Mechatronics* 31 (2015), pp. 116–123. DOI: 10.1016/j.mechatronics.2015.03.008.

[14] Petter Hagqvist et al. “Resistance measurements for control of laser metal wire deposition.” In: *Optics and Lasers in Engineering* 54 (2014), pp. 62–67. DOI: 10.1016/j.optlaseng.2013.10.010.

[15] P. K. C. Kanigalpula et al. “Experimental investigations, input-output modeling and optimization for electron beam welding of Cu-Cr-Zr alloy plates.” In: *The International Journal of Advanced Manufacturing Technology* 85.1-4 (2015), pp. 711–726. DOI: 10.1007/s00170-015-7964-7.

[16] P. Rajesh Kannan, V. Muthupandi, and K. Devakumaran. “On the effect of temperature coefficient of surface tension on shape and geometry of weld beads in hot wire gas tungsten arc welding process.” In: *Materials Today: Proceedings* 5.2 (2018), pp. 7845–7852. DOI: 10.1016/j.matpr.2017.11.465.

[17] Christian Kledwig et al. “Analysis of Melt Pool Characteristics and Process Parameters Using a Coaxial Monitoring System during Directed Energy Deposition in Additive Manufacturing.” In: *Materials* 12.2 (2019), p. 308. DOI: 10.3390/ma12020308.

[18] Michael Kottman et al. “Laser Hot Wire Process: A Novel Process for Near-Net Shape Fabrication for High-Throughput Applications.” In: *Jom* 67.3 (2015), pp. 622–628. DOI: 10.1007/s11837-014-1288-1.

[19] Yongzhe Li et al. “Interlayer closed-loop control of forming geometries for wire and arc additive manufacturing based on fuzzy-logic inference.” In: *Journal of Manufacturing Processes* 63 (2021), pp. 35–47. DOI: 10.1016/j.jmapro.2020.04.009.

[20] Wei Liu et al. “Real-time monitoring of the laser hot-wire welding process.” In: *Optics & Laser Technology* 57 (2014), pp. 66–76. DOI: 10.1016/j.optlastec.2013.09.026.

[21] Tatiana V. Olshanskaya et al. “Electron beam welding of aluminum alloy AlMg6 with a dynamically positioned electron beam.” In: *The International Journal of Advanced Manufacturing Technology* 89.9-12 (2016), pp. 3439–3450. DOI: 10.1007/s00170-016-9316-7.

[22] R H Phillips and E A Metzbower. “Laser Beam Welding of HY80 and HY100 Steels Using Hot Welding Wire Addition.” In: *Welding Journal* (June 1992), 201-s-208–s. URL: files.aws.org.

[23] *Process Capability (Cp, Cpk) and Process Performance (Pp, Ppk) - What is the Difference?* Nov. 2018. URL: https://www.isixsigma.com/tools-templates/capability-indices-process-capability/process-capability-cp-cpk-and-process-performance-pp-ppk-what-difference/.

[24] Aljaž Ščetinec, Damjan Klobčar, and Drago Bračun. "In-process path replanning and online layer height control through deposition arc current for gas metal arc based additive manufacturing." In: *Journal of Manufacturing Processes* 64 (2021), pp. 1169–1179. DOI: 10.1016/j.jmapro.2021.02.038.

[25] Federico Sciammarella and Benyamin Salehi Najafabadi. "Processing Parameter DOE for 316L Using Directed Energy Deposition." In: *Journal of Manufacturing and Materials Processing* 2.3 (2018), p. 61. DOI: 10.3390/jmmp2030061.

[26] Kevin Michael Scott and Richard Martin Hutchison. "Hotwire deposition material processing system and method." en. US20150083702A1. Mar. 2015. URL: https://patents.google.com/patent/US20150083702A1/en (visited on 07/11/2021).

[27] David Svetlizky et al. "Directed energy deposition (DED) additive manufacturing: Physical characteristics, defects, challenges and applications." In: *Materials Today* (2021). DOI: 10.1016/j.mattod.2021.03.020.

[28] Blanka A. Szost et al. "A comparative study of additive manufacturing techniques: Residual stress and microstructural analysis of CLAD and WAAM printed Ti–6Al–4V components." en. In: *Materials & Design* 89 (Jan. 2016), pp. 559–567. ISSN: 02641275. DOI: 10.1016/j.matdes.2015.09.115. URL: https://linkinghub.elsevier.com/retrieve/pii/S0264127515305268 (visited on 06/29/2021).

[29] Shigeru Takushima et al. "Optical in-process height measurement system for process control of laser metal-wire deposition." en. In: *Precision Engineering* 62 (Mar. 2020), pp. 23–29. ISSN: 01416359. DOI: 10.1016/j.precisioneng.2019.11.007. URL: https://linkinghub.elsevier.com/retrieve/pii/S0141635919307706 (visited on 06/29/2021).

[30] Dieter Tyralla and Thomas Seefeld. "Temperature field based closed-loop control of laser hot wire cladding for low dilution." en. In: *Procedia CIRP* 94 (2020), pp. 451–455. ISSN: 22128271. DOI: 10.1016/j.procir.2020.09.163. URL: https://linkinghub.elsevier.com/retrieve/pii/S2212827120313512 (visited on 06/29/2021).

[31] Daniel René Tasé Velázquez et al. "Prediction of Geometrical Characteristics and Process Parameter Optimization of Laser Deposition AISI 316 Steel Using Fuzzy Inference." In: (2021). DOI: 10.21203/rs.3.rs-296663/v1.

[32] T.r. Walker et al. "A novel numerical method to predict the transient track geometry and thermomechanical effects through in-situ modification of the process parameters in Direct Energy Deposition." In: *Finite Elements in Analysis and Design* 169 (2020), p. 103347. DOI: 10.1016/j.finel.2019.103347.

[33] Samantha Webster, Kornel Ehmann, and Jian Cao. "Energy Density Comparison via Highspeed, In-situ Imaging of Directed Energy Deposition." In: *Procedia Manufacturing* 48 (2020), pp. 691–696. DOI: 10.1016/j.promfg.2020.05.101.

[34] Haiying Wei et al. “Energy efficiency evaluation of hot-wire laser welding based on process characteristic and power consumption.” In: *Journal of Cleaner Production* 87 (2015), pp. 255–262. DOI: 10.1016/j.jclepro.2014.10.009.

VITA

Christopher Michael Croft began his work as an undergraduate research assistant under Dr. Frank Liou in April of 2018. He received his Bachelor of Science degree in Mechanical Engineering from Missouri University of Science and Technology in May, 2020. He then continued research under Dr. Frank Liou while pursuing his master's degree. He received his Master of Science degree in Manufacturing Engineering from Missouri University of Science and Technology in December 2021.